Molecular Dynamics

DOI: 10.1002/ange.201307822

Resonances in the Entrance Channel of the Elementary Chemical Reaction of Fluorine and Methane**

*Till Westermann, Jongjin B. Kim, Marissa L. Weichman, Christian Hock, Tara I. Yacovitch, Juliana Palma, Daniel M. Neumark, and Uwe Manthe**

Abstract: *Extending the fully quantum-state-resolved description of elementary chemical reactions beyond three or four atom systems is a crucial issue in fundamental chemical research. Reactions of methane with F, Cl, H or O are key examples that have been studied prominently. In particular, reactive resonances and nonintuitive mode-selective chemistry have been reported in experimental studies for the $F + CH_4 \rightarrow HF + CH_3$ reaction. By investigating this reaction using transition-state spectroscopy, this joint theoretical and experimental study provides a clear picture of resonances in the $F + CH_4$ system. This picture is deduced from high-resolution slow electron velocity-map imaging (SEVI) spectra and accurate full-dimensional (12D) quantum dynamics simulations in the picosecond regime.*

Fundamental research on elementary chemical reactions has achieved a fully quantum-state-resolved level of understanding for triatomic and, more recently, for tetra-atomic reactions. Extending this understanding towards larger systems, recent research has focused on bimolecular reactions of methane with F, Cl, H or O as benchmark examples. Experimental studies have revealed mode-selective chemistry in these systems and observed signatures of reactive resonances.[1–9] To interpret and comprehend these phenomena, theoretical research is necessary. Full-dimensional potential-energy surfaces (PESs) based on high-level ab initio calculations have been constructed,[8,10–12] and quantum-state-resolved reaction dynamics on these surfaces have been studied by quasi-classical trajectory simulations, which cannot describe resonances[4,11–13] and reduced-dimensional wave-packet calculations.[8,14,15] Rigorous full-dimensional quantum dynamics calculations studying these six-atom reactions on accurate PESs were restricted to short simulation times of a few tens of femtoseconds and typically computed thermal rate constants.[16]

The $F + CH_4 \rightarrow HF + CH_3$ reaction is particularly interesting as a prototypical example of an early barrier reaction. It shows a low barrier of 3.23 kJ mol^{-1} with a bent transition state that partially inherits its structure from the van der Waals complex present in the entrance channel of the reaction. Studying the mode-selective chemistry of the $F + CHD_3$ reaction,[3,4] the van der Waals complex was found to severely influence the reaction dynamics: it results in, for example, a counterintuitive effect of H–C stretching excitation on the $HF + CD_3/DF + CHD_2$ branching ratio. To provide detailed information on the dynamics in the vicinity of the reaction barrier, the $F + CH_4 \rightarrow HF + CH_3$ reaction using photodetachment of CH_4F^- was investigated by spectroscopic experiments.[17,18] Prominent resonance structures were detected in the high-resolution photodetachment spectra but could not be assigned.[18] The present work provides a detailed picture explaining these structures and the underlying quantum dynamics. To this end, rigorous full-dimensional (12D) wave-packet calculations studying the quantum dynamics of the $F + CH_4$ system after the photodetachment of CH_4F^- on a picosecond time scale will be presented and compared with new, high-resolution experimental results.

Transition-state spectroscopy[19] probes the dynamics in the vicinity of the transition state using photodetachment of an ionic precursor. In the present case, an electron is detached from CH_4F^- to obtain the reactive species. CH_4F^- effectively shows a C_{3v}-symmetric structure where the fluorine atom is located close to one hydrogen atom at a linear C–H···F arrangement (see inset (b) of Figure 1 for a schematic representation of the geometry).[20,21] The Franck–Condon point of the photodetachment process is located in the entrance channel of the $F + CH_4 \rightarrow HF + CH_3$ reaction close to the transition state of the reaction. Following electron detachment, the wave packet evolves on the PESs of the neutral $F + CH_4$ system. A schematic plot of the PESs is given in Figure 1. The present work employs a newly developed set of six vibronically and spin–orbit-coupled PESs (see the Computational and Experimental Section for details) to describe the three doubly degenerate electronic states which are relevant for the process. In the entrance channel of the reaction, different van der Waals minima are found depend-

[*] T. Westermann, Prof. Dr. U. Manthe
Theoretische Chemie, Fakultät für Chemie
Universität Bielefeld, Universitätsstr. 25
33615 Bielefeld (Germany)
E-mail: uwe.manthe@uni-bielefeld.de
J. B. Kim, M. L. Weichman, Dr. C. Hock, Dr. T. I. Yacovitch, Prof. Dr. D. M. Neumark
Department of Chemistry, University of California
Berkeley, CA 94720 (USA)
Prof. Dr. J. Palma
Departamento de Ciencia y Tecnología
Universidad Nacional de Quilmes, Sáenz Peña 352
Bernal B1876BXD (Argentina)

[**] The experimental part of this research is funded by the Air Force Office of Scientific Research under grant number FA9550-12-1-0160 and the Defense University Research Instrumentation Program under grant number FA9550-11-1-0300. M.L.W. thanks the National Science Foundation for a graduate research fellowship. For the theoretical part, financial support by the Deutsche Forschungsgemeinschaft and the Alexander von Humboldt Foundation is gratefully acknowledged.

Supporting information for this article is available on the WWW under http://dx.doi.org/10.1002/anie.201307822.

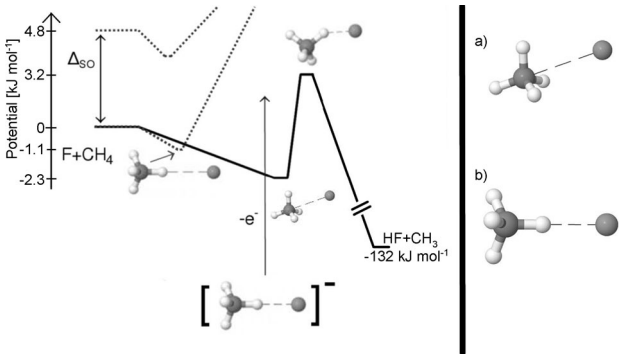

Figure 1. Left-hand side: Schematic overview of the PESs involved in the $CH_4 + F \rightarrow FH + CH_3$ reaction (top). The solid potential curve indicates the reactive A_1 state and the dotted potential curves the nonreactive *E* states. Δ_{SO} is the atomic spin–orbit splitting. The arrow, marked with e^-, indicates the initial state generated by detaching an electron from the anionic CH_4F^- precursor complex. Right-hand side: a) H–C···F equilibrium geometry of the van der Waals complex. b) H_3C–H···F geometry at the Franck–Condon point.

ing on the electronic state. The most prominent minima are found at C_{3v}-symmetric geometries where the fluorine is located opposite to a hydrogen atom at H–CH_3···F (see inset (a) of Figure 1 for a schematic representation of this geometry).

Photodetachment spectra for CH_4F^- and CD_4F^- are given in Figures 2 and 3. The experimental spectra are obtained by slow electron velocity-map imaging (SEVI) of cryogenically cooled ions and the theoretical spectra are calculated by converged full-dimensional quantum dynamics on six coupled PESs employing the multi-configurational time-dependent Hartree (MCTDH) approach[24,25] (see the Computational and Experimental Section for details). The photon used in the SEVI overview spectrum (307 nm for CH_4F^- and 315 nm for CD_4F^-, respectively) are very close to the threshold for photodetachment. Consequently, the measured peak intensities can deviate from the idealized theoretical spectrum which assumes instantaneous electron detachment.

Overview low-resolution spectra for both isotopic species are shown in Figure 2 and show two main peaks. The first peak centered around 30000 cm^{-1} is due to transitions to the ground electronic state (labeled A). The second, broader peak, centered around 31250 cm^{-1}, results predominantly from transitions to the excited electronic states (labeled E). In previous work,[26] it was found theoretically that excitation into the nonreactive E states is followed by a fast and complete dissociation into $CH_4 + F$. This leads to a broad peak in the spectrum. Photodetachment to the reactive A state, which is less repulsive, results in a sharper peak.[27] This peak is further investigated by high-resolution experimental and theoretical photodetachment spectra.

High-resolution spectra for both isotopic species are shown in Figure 3. In the energy regime between 29500 and 30000 cm^{-1}, both the CH_4F^- and CD_4F^- spectra are highly structured. The structure in the CH_4F^- experimental spectra is consistent with that reported previously,[18] but the CD_4F^- spectra resolve a progression that was not observed in the previous experiment. Improvements to the photoelectron spectroscopy apparatus have increased experimental resolution and sensitivity,[35] allowing the observation of an analogous progression in both species. For CH_4F^- the experimental data show peak spacings between 15–25 cm^{-1} and an average progression of 19 cm^{-1} is found in the theoretical calculation. For CD_4F^-, typical peak spacings of 15–20 cm^{-1} are found experimentally, compared to 16 cm^{-1} in the theoretical calculations. The very similar progressions and the agreement in the low-resolution spectra indicate that the essential processes present in the system are described by the theoretical calculations. Therefore, the theoretical calcula-

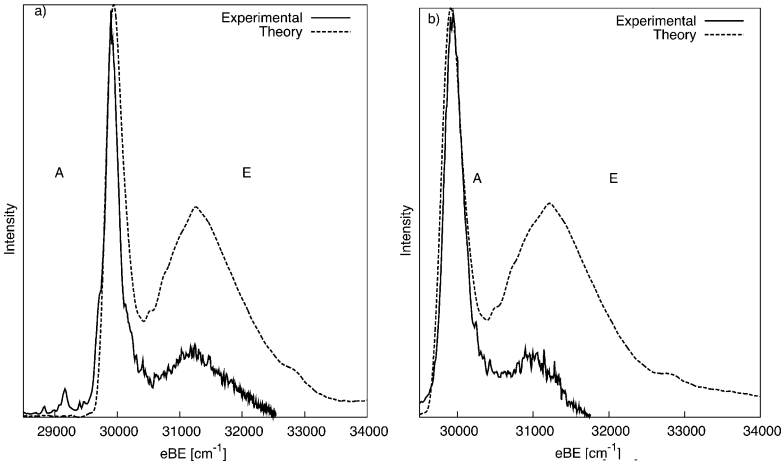

Figure 2. Photodetachment overview spectra for a) CH_4F^- and b) CD_4F^-. The experimental spectra were obtained at 315 and 307 nm, respectively. See the Computational and Experimental Section for details.

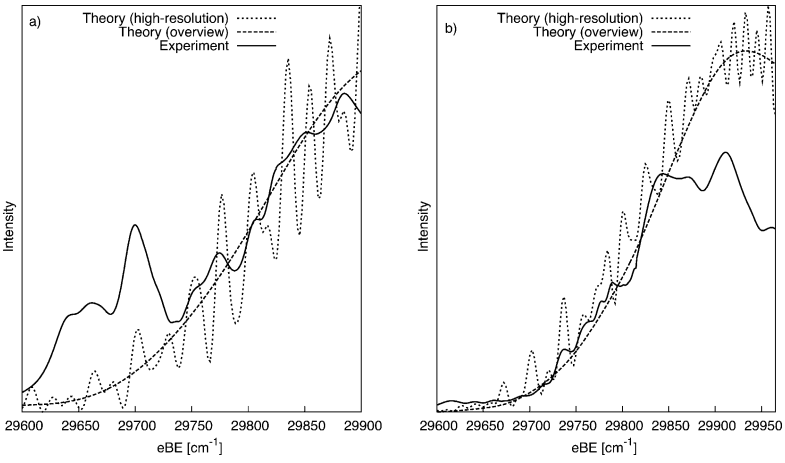

Figure 3. High-resolution photodetachment spectra for a) CH_4F^- and b) CD_4F^-. See the Computational and Experimental Section for details.

tions can be used to understand the underlying processes in detail.

As explained above, the initial nuclear wave function is inherited from the anionic precursor, which is centered at a linear F–H–CH_3 geometry. After the electron is detached, the wave packet propagates on the PESs of the neutral F + CH_4 system, which shows potential minima at bent geometries as well as open channels toward dissociation in F + CH_4 reactants and HF + CH_3 products. To gain a deeper understanding for the process of the reactive A state, the time-dependent wave function obtained from the quantum dynamics simulation, which contains all information about the system, is analyzed (see the Supporting Information). From this, we can draw the following picture.

Two dominant motions are found, the F···CH_4 stretching motion and a relative rotation of fluorine and methane with respect to each other. In the first 200 fs after the electron is detached, the relative rotation of methane and fluorine is found to be faster than the dissociation into F + CH_4 because of the low moments of inertia of CH_4. In the first 100 fs, the systems rotates from a pseudo-linear H_3C–H···F geometry (as depicted in inset (b) of Figure 1) to the neighboring minima of the van der Waals complex, which show a H–CH_3···F arrangement (as depicted in inset(a) of Figure 1). The majority of the wave function continues to rotate and performs a 180° rotation after about 160 fs. Dissociation only plays a minor role during this period. Having gained momentum towards the dissociation into F + CH_4, relevant parts of the wave function start to dissociate for times longer than 200 fs. For these parts, very complex and chaotic dynamics are observed, including large amplitude motions where some parts of the wave function are trapped very close to the dissociation threshold.

Having discussed the main process above, the physics contributing to the fine structure is discussed. As pointed out above, the Franck–Condon point of the system shows a nearly linear H_3C–H···F geometry and the relative rotation of the fluorine atom and the methane molecule with respect to each other is the dominant motion in the first 200 fs. The wave function is performing a rotation to the neighboring H–CH_3···F minima in the first 100 fs. At this point, minor parts of the wave function do not continue to rotate because they are reflected at the neighboring hydrogen atoms, which are located in the direction of the rotation. These hydrogen atoms provide an atomic post for the reflection, which stops the rotation. The reflected parts of the wave function return to the Franck–Condon point and induce recurrences, which are responsible for the observed fine structure.

In the autocorrelation function, multiple recurrences are found, a first weak recurrence at 400 fs and a stronger one at 660 fs. Further recurrences follow for later times (see the Supporting Information). In contrast to the photodetachment spectra of triatomic systems as H_2F^-, where isolated resonances were found and quantum numbers could be assigned,[28] the high density of states and chaotic dynamics prohibit such analysis for the present system. Here an analysis based on periodic orbits (see, e.g., Ref. [29] for a review on the subject) allows one to identify the characteristic motions which cause the resonance structures. Prototypical periodic orbits starting in the vicinity of the Franck–Condon region are shown in Figure 4. They correspond to the recurrences described above and represent periodic motions with time periods of 330 (a) and 700 fs (b), respectively. The trajectories depict a motion where the fluorine atom is moving back and forth between two hydrogen atoms of the methane molecule. This motion is found to be significantly coupled to the CH_4-F stretching motion. In the wave function, these recurrences form resonances that are stable for longer than 1.5 ps.

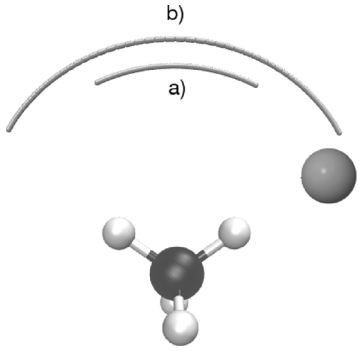

Figure 4. Classical periodic orbits corresponding to the recurrences found in the autocorrelation function. The time for one periodic motion is a) 330 and b) 700 fs, respectively.

In the case of CD_4F^-, the behavior is similar although slightly more complex. Because of the isotope effect, the relative rotation becomes slower by a factor of $\sqrt{2}$ while the effect on the CH_4-F stretch is not as drastic (a factor of $\sqrt{(39/35)}$). Thus, the relative rotation and the dissociation into F + CD_4 happen on more similar time scales, resulting in less separability.

In conclusion, accurate full-dimensional wave-packet dynamics calculations studying resonance structures in the entrance channel and the transition-state region of the F + CH_4 → HF + CH_3 reaction by simulations on a picosecond time scale have been reported and compared to improved experimental spectra. The calculations employ a newly developed set of diabatic PESs, which accurately describe the vibronic and spin–orbit coupling present in the entrance channel of the reaction. Good agreement is found between the theoretical results and improved transition-state spectroscopy measurements. The present results highlight the importance of pre-reactive van der Waals complexes for the F + CH_4 → HF + CH_3 reaction. In this distinctly early barrier reaction, quasi-bound states of the pre-reactive van der Waals complex show significant overlap with the transition-state region and resonance structures can be seen in the transition-state spectra. Both theory and experiment confirm a high density of such quasi-bound states. These states are likely to mediate the reaction of F + CH_4 → HF + CH_3 at low temperatures and give rise to complex steering effects which already have been detected in scattering experiments studying the control of chemical reactivity by laser excitation of specific vibrations.[3]

Computational and Experimental Section

Theory: Coupled diabatic PESs for $F + CH_4$ have been constructed following the approach of Ref. [26]. For the description of the excited electronic states as well as for geometries with C–F distances larger than 3.6 Å, the data obtained by multi-reference configuration interactions (MRCI) were taken from Ref. [26]. To improve the accuracy of the ground-state PESs compared to Ref. [26], new ab initio results obtained by explicitly correlated coupled cluster calculations on the UCCSD(T)-F12a level with an aug-cc-pvtz basis using the MOLPRO program[30] were employed to describe the electronic ground state at smaller C–F distances. The wave-packet dynamics calculations were performed using the MCTDH approach[24,25] and the correlation discrete variable representation (CDVR) potential quadrature.[31] The basis set sizes required to obtain convergence are described in the Supporting Information. The calculation of the initial wave packet and the low-resolution spectra followed the approach used in previous work.[26,27] In the calculation of the high-resolution spectrum, the initial wave packet generated by the photodetachment was first propagated in an imaginary time for $\beta = 4000$ a.u. before the real-time propagation was started. The photodetachment spectra were obtained by Fourier transforming the autocorrelation function and multiplying the resulting raw spectrum by an appropriate energy-dependent factor to compensate for the effect of the imaginary time propagation. This procedure crucially improves the energy resolution in the low-energy regime. Autocorrelation function data was calculated up to a time $t = 2.0$ ps and the $\cos^2$-filter described in Ref. [32] was employed to avoid noise resulting from the limited propagation time. All spectra are shifted by $-10\ cm^{-1}$ to improve the agreement with the experimental data.

Experiment: The SEVI anion photoelectron apparatus has been described in detail previously.[33–35] SEVI uses an electron imaging spectrometer at low extraction voltages, allowing for an expanded view of the low kinetic energy electrons and a sub-milli electron volt energy resolution. The low-resolution overview experimental spectra of Figure 2 are from Ref. [18] but the high-resolution spectra of Figure 3 make use of ion cooling and photoelectron event counting. The instrumental resolution is the same as in the previous experiment. However, the addition of photoelectron event counting for the imaging detector allows for improved sensitivity and signal-to-noise. In addition, ion temperatures are unknown for the previous experiment, but rotational substructure and vibrational hot bands may contribute to the spectral congestion. Ion trapping and cooling is expected to minimize such effects by cooling the anions to a temperature of about 10 K before photodetachment. A gas mixture of trace NF_3 and 10% CH_4/CD_4 in helium was expanded through a pulsed valve into the vacuum. F^- was generated by dissociative electron attachment to NF_3 by a pulsed ring ionizer, and CH_4F^-/CD_4F^- complexes were stabilized in the jet expansion. The ions were stored in an radio frequency (RF) ion trap and cooled by a 20:80 H_2:He buffer gas mix at 5 K. The ions were extracted from the trap, mass-selected, and photodetached by the frequency-doubled output of a tunable dye laser. The electron kinetic energy distributions are reconstructed with the BASEX algorithm, and the electron binding energy (eBE) spectra derived by subtracting the electron kinetic energy (eKE) from the photon energy.[36] As the low-eKE segments of each spectrum have the highest resolution, the experimental spectra presented are composites made from segments of spectra taken at different wavelengths, spliced together, and scaled to match the overview spectra. Peak intensities are not definitive because of the composite nature and threshold intensity effects of the Wigner threshold law,[37] but peak positions are expected to be accurate to within $4\ cm^{-1}$.

The spectra are plotted with respect to the electron binding energy, defined as the difference between the photodetachment photon energy and the measured electron kinetic energy.

Received: September 5, 2013
Published online: December 4, 2013

Keywords: ab initio calculations · molecular dynamics · photoelectron spectroscopy · potential-energy surfaces · van der Waals complexes

[1] J. Lin, J. Zhou, W. Shiu, K. Liu, *Science* **2003**, *300*, 966–969.
[2] W. Shiu, J. Lin, K. Liu, *Phys. Rev. Lett.* **2004**, *92*, 103201.
[3] W. Zhang, H. Kawamata, K. Liu, *Science* **2009**, *325*, 303–306.
[4] G. Czakó, Q. Shuai, K. Liu, J. M. Bowman, *J. Chem. Phys.* **2010**, *133*, 131101.
[5] S. Yan, Y.-T. Wu, B. Zhang, X.-F. Yue, K. Liu, *Science* **2007**, *316*, 1723–1726.
[6] S. Yan, Y.-T. Wu, B. Zhang, X.-F. Yue, K. Liu, *Proc. Natl. Acad. Sci. USA* **2008**, *105*, 12667–12672.
[7] F. Wang, J.-S. Lin, K. Liu, *Science* **2011**, *331*, 900–903.
[8] W. Zhang, Y. Zhou, G. Wu, Y. Lu, H. Pan, B. Fu, Q. Shuai, L. Liu, S. Liu, L. Zhang, B. Jiang, D. Dai, S. Lee, Z. Xie, B. Braams, J. Bowman, M. Collins, D. Zhang, X. Yang, *Proc. Natl. Acad. Sci. USA* **2010**, *107*, 12782–12785.
[9] F. Wang, K. Liu, *Chem. Sci.* **2010**, *1*, 126–133.
[10] G. Czakó, B. C. Shepler, B. J. Braams, J. M. Bowman, *J. Chem. Phys.* **2009**, *130*, 084301.
[11] G. Czakó, J. M. Bowman, *Science* **2012**, *334*, 343–346.
[12] G. Czakó, J. M. Bowman, *Proc. Natl. Acad. Sci. USA* **2012**, *109*, 7997–8001.
[13] G. Czakó, J. M. Bowman, *J. Am. Chem. Soc.* **2009**, *131*, 17534–17535.
[14] Z. Zhang, Y. Zhou, D. H. Zhang, G. Czakó, J. M. Bowman, *J. Phys. Chem. Lett.* **2012**, *3*, 3416–3419.
[15] S. Liu, J. Chen, Z. Zhang, D. H. Zhang, *J. Chem. Phys.* **2013**, *138*, 011101.
[16] T. Wu, H.-J. Werner, U. Manthe, *Science* **2004**, *306*, 2227–2229.
[17] M. Cheng, Y. Feng, Y. Du, Q. Zhu, W. Zheng, G. Czakó, J. M. Bowman, *J. Chem. Phys.* **2011**, *134*, 191102.
[18] T. I. Yacovitch, E. Garand, J. B. Kim, C. Hock, T. Theis, D. M. Neumark, *Faraday Discuss.* **2012**, *157*, 399–414.
[19] D. M. Neumark, *Phys. Chem. Chem. Phys.* **2005**, *7*, 433–442.
[20] G. Czakó, B. J. Braams, J. M. Bowman, *J. Phys. Chem. A* **2008**, *112*, 7466–7472.
[21] R. Wodraszka, J. Palma, U. Manthe, *J. Phys. Chem. A* **2012**, *116*, 11249–11259.
[22] H. Wang, M. Thoss, *J. Chem. Phys.* **2003**, *119*, 1289–1299.
[23] U. Manthe, *J. Chem. Phys.* **2008**, *128*, 164116.
[24] H.-D. Meyer, U. Manthe, L. S. Cederbaum, *Chem. Phys. Lett.* **1990**, *165*, 73–78.
[25] U. Manthe, H.-D. Meyer, L. S. Cederbaum, *J. Chem. Phys.* **1992**, *97*, 3199–3213.
[26] T. Westermann, W. Eisfeld, U. Manthe, *J. Chem. Phys.* **2013**, *139*, 014309.
[27] J. Palma, U. Manthe, *J. Chem. Phys.* **2012**, *137*, 044306.
[28] D. E. Manolopoulos, K. Stark, H.-J. Werner, D. W. Arnold, S. E. Bradforth, D. M. Neumark, *Science* **1993**, *262*, 1852–1855.
[29] I. Llorente, E. Pollak, *Annu. Rev. Phys. Chem.* **1992**, *43*, 91–126.
[30] MOLPRO, version 2009.1, is a package of ab initio programs written by H.-J. Werner and P. J. Knowles, with contributions from R. D. Amos, A. Berning, D. L. Cooper, M. J. O. Deegan, A. J. Dobbyn, F. Eckert, C. Hampel, G. Hetzer, T. Leininger, R. Lindh, A. W. Lloyd, W. Meyer, M. E. Mura, A. Nicklaß, P.

Palmieri, K. Peterson, R. Pitzer, P. Pulay, G. Rauhut, M. Schütz, H. Stoll, A. J. Stone and T. Thorsteinsson.
[31] U. Manthe, *J. Chem. Phys.* **1996**, *105*, 6989 – 6994.
[32] H.-D. Meyer, F. Gatti, G. A. Worth, *Multidimensional Quantum Dynamics: MCTDH Theory and Applications*, Weinheim, Wiley-VCH, **2009**.
[33] A. Osterwalder, M. J. Nee, J. Zhou, D. M. Neumark, *J. Chem. Phys.* **2004**, *121*, 6317 – 6322.
[34] D. M. Neumark, *J. Phys. Chem. A* **2008**, *112*, 13287 – 13301.
[35] C. Hock, J. B. Kim, M. L. Weichman, T. I. Yacovitch, D. M. Neumark, *J. Chem. Phys.* **2012**, *137*, 244201.
[36] V. Dribinski, A. Ossadtchi, V. A. Mandelshtam, H. Reisler, *Rev. Sci. Instrum.* **2002**, *73*, 2634 – 2642.
[37] E. P. Wigner, *Phys. Rev.* **1948**, *73*, 1002 – 1009.
[38] C. Evenhuis, G. Nyman, U. Manthe, *J. Chem. Phys.* **2007**, *127*, 144302.
[39] G. Schiffel, U. Manthe, *Chem. Phys.* **2010**, *374*, 118 – 125.
[40] D. Kosloff, R. Kosloff, *J. Comput. Phys.* **1983**, *52*, 35 – 53.
[41] D. O. Harris, G. G. Engerholm, W. D. Gwinn, *J. Chem. Phys.* **1965**, *43*, 1515.
[42] A. S. Dickinson, P. R. Certain, *J. Chem. Phys.* **1968**, *49*, 4209 – 4211.
[43] J. C. Light, I. P. Hamilton, J. V. Lill, *J. Chem. Phys.* **1985**, *82*, 1400 – 1409.

